


ORIGINAL ARTICLE

Open Access



# An Automatic Implementation of Oropharyngeal Swab Sampling for Diagnosing Respiratory Infectious Diseases via Soft Robotic End-Effectors

Yafeng Cui<sup>1</sup>, Wenjie Yu<sup>2</sup>, Jingjing Li<sup>3</sup>, Qi Shao<sup>1</sup>, Ding Weng<sup>1</sup>, Guoping Yin<sup>3</sup>, Xiaohao Zhang<sup>4</sup>, Xinjun Liu<sup>1</sup>, Jingying Ye<sup>3\*</sup>, Jiadao Wang<sup>1\*</sup> and Huichan Zhao<sup>1\*</sup> 

## Abstract

The most widely adopted method for diagnosing respiratory infectious diseases is to conduct polymerase chain reaction (PCR) assays on patients' respiratory specimens, which are collected through either nasal or oropharyngeal swabs. The manual swab sampling process poses a high risk to the examiner and may cause false-negative results owing to improper sampling. In this paper, we propose a pneumatically actuated soft end-effector specifically designed to achieve all of the tasks involved in swab sampling. The soft end-effector utilizes circumferential instability to ensure grasping stability, and exhibits several key properties, including high load-to-weight ratio, error tolerance, and variable swab-tip stiffness, leading to successful automatic robotic oropharyngeal swab sampling, from loosening and tightening the transport medium tube cap, holding the swab, and conducting sampling, to snapping off the swab tail and sterilizing itself. Using an industrial collaborative robotic arm, we integrated the soft end-effector, force sensor, camera, lights, and remote-control stick, and developed a robotic oropharyngeal swab sampling system. Using this swab sampling system, we conducted oropharyngeal swab-sampling tests on 20 volunteers. Our Digital PCR assay results (RNase P RNA gene absolute copy numbers for the samples) revealed that our system successfully collected sufficient numbers of cells from the pharyngeal wall for respiratory disease diagnosis. In summary, we have developed a pharyngeal swab-sampling system based on an "enveloping" soft actuator, studied the sampling process, and implemented whole-process robotic oropharyngeal swab-sampling.

**Keywords** Diagnosis, Medical robot, Soft end-effector, Swab-sampling, Digital PCR

\*Correspondence:

Jingying Ye  
yejingying@mail.tsinghua.edu.cn  
Jiadao Wang  
jdwang@mail.tsinghua.edu.cn  
Huichan Zhao  
zhaohuichan@mail.tsinghua.edu.cn

<sup>1</sup> Department of Mechanical Engineering, Tsinghua University, Beijing 100084, China

<sup>2</sup> Beijing Huakang Tongbang Technology Company, Beijing 102609, China

<sup>3</sup> Department of Otorhinolaryngology, Beijing Tsinghua Changgung Hospital, School of Clinical Medicine, Tsinghua University, Beijing 102218, China

<sup>4</sup> Tianjin Research Institute for Advanced Equipment, Tsinghua University, Tianjin 300300, China



© The Author(s) 2024. **Open Access** This article is licensed under a Creative Commons Attribution 4.0 International License, which permits use, sharing, adaptation, distribution and reproduction in any medium or format, as long as you give appropriate credit to the original author(s) and the source, provide a link to the Creative Commons licence, and indicate if changes were made. The images or other third party material in this article are included in the article's Creative Commons licence, unless indicated otherwise in a credit line to the material. If material is not included in the article's Creative Commons licence and your intended use is not permitted by statutory regulation or exceeds the permitted use, you will need to obtain permission directly from the copyright holder. To view a copy of this licence, visit <http://creativecommons.org/licenses/by/4.0/>.

## 1 Introduction

Since the end of 2019, a severely infectious respiratory disease, Coronavirus Disease 2019 (COVID-19), has spread globally, infecting hundreds of millions of people and caused millions of deaths [1–3]. Respiratory infections are difficult to identify in the population, as the typical symptoms (e.g., fever, cough, sore throat, and fatigue) can be rather mild, appearing several days after exposure to the virus; nonetheless, patients with mild infections can still spread the virus [4, 5]. In addition, asymptomatic transmission can occur [6]. Therefore, an accurate, convenient, and easily implemented method for diagnosing infectious respiratory disease is essential to prevent its spread [7].

Currently, the most widely adopted method for diagnosing infectious respiratory diseases such as COVID-19 and Influenza A is to conduct polymerase chain reaction (PCR) assays on patients' respiratory specimens, which are collected through either nasal or oropharyngeal swabs [7–9]. Nasal or oropharyngeal swab sampling procedures are usually performed by experienced examiners who are fully protected by gear such as masks, gloves, gowns, and goggles, to prevent themselves from being infected by the virus during the process. However, even when well protected, examiners still face risks of infection from unexpected contact, droplets, and exhaled air from patients with suspected infectious respiratory disease. Due to the infectious respiratory disease outbreak, the need for nasal or oropharyngeal swab sampling is increasing substantially, thereby also increasing examiners' workload and mental stress and potentially increasing their risk [10]. This simultaneously causes lower sensitivity and accuracy of the PCR testing due to reduced amount of the cells being collected [11].

Robotic equipment has the potential to perform manual sampling tasks and spatially isolate suspected infectors from examiners [12–14]. Robotic implementation holds advantages over manual implementation. First, the examiner's risk of viral exposure could be reduced to zero. Second, the robots perform sampling with repeatable contours, controllable forces, and stable speeds, potentially producing specimens with higher PCR test accuracy. Promising as it is, there are still challenges in robotic swab-sampling. In manual testing, examiners perform the following tasks gently and effectively, and with dexterity: manipulating the swabs and viral transport medium (VTM) tubes and caps; screwing and unscrewing the caps; rotating the swabs and rubbing them along the back of the throat; and snapping off the end of the swab. These tasks involve exceptional human capabilities, including dexterous multi-finger manipulation, accurate motor control, sensitivity to force- and visual-feedback, and intelligent hand-eye coordination.

In recent years, soft robots [15–18] have developed rapidly, owing to their safe interaction with humans [19–21], high environmental adaptability [22, 23], and satisfactory performance in both manipulation [15–17, 24–26] and locomotion [27–30]. In terms of soft manipulation, many smart soft end-effectors have been proposed for grasping various objects [31, 32]. Soft end-effectors are usually lightweight, safe, and adaptive to object shape and softness [33–36]. Amend et al. developed a granular gripper that can quickly grasp and release irregular objects through positive and negative pressure adjustment [37]. Sinatra et al. proposed an underwater gripper that can be used to grab fragile marine organisms such as jellyfish [38]. Li et al. have developed a vacuum-driven origami gripper that is highly adaptive to daily objects [39]. Xie et al. incorporated vacuum suckers into a tapered octopus-arm-inspired gripper to enhance its gripping ability [25]. Robotics Inc. has produced soft grippers that can sort goods on production lines and handle soft and delicate objects such as food [40]. OnRobot A/S has developed a cup-shaped, food-grade soft gripper that can easily handle irregular shapes and delicate objects [41]. Wang et al. presented a pneumatic soft robotic gripper that consists of a cylindrical soft actuator and a detachable sucker, to achieve high load capacity and large grasping range [42]. Although the various soft end-effectors can handle a large variety of objects, swab manipulation and sampling remain challenging because they require the end-effectors to small as well as designed for high load and high safety procedures, high force controllability, and precise positional alignment during automatic sampling. The question of how to collect specimens effectively and safely from humans using robots has not been well addressed [43].

In this work, we have adopted an “enveloping” grasping strategy [37–39, 44–47] and developed a pneumatically actuated soft end-effector specifically designed for achieving all of the tasks involved in oropharyngeal swab sampling (Figure 1). Figure 1(a) shows the robotic swab-sampling system collecting a sample from a volunteer (inset: Diagram of the end-effector holding an oropharyngeal swab). Figure 1(b) shows the soft end-effector loosening or tightening the VTM tube cap. Figure 1(c) shows the soft end-effector holding a swab and preparing for sample collection. Figure 1(d) shows the soft end-effector snapping off the swab tail. The soft end effector utilizes circumferential instability to ensure grasping stability, and exhibits several key properties, including high load-to-weight ratio (up to 315 load-to-weight ratio, and 24.52 N·m/kg torque-to-weight ratio), error tolerance (up to 6 mm misalignment), and variable stiffness (up to twice of the swab's baseline stiffness). Based on these features, automatic robotic oropharyngeal swab sampling

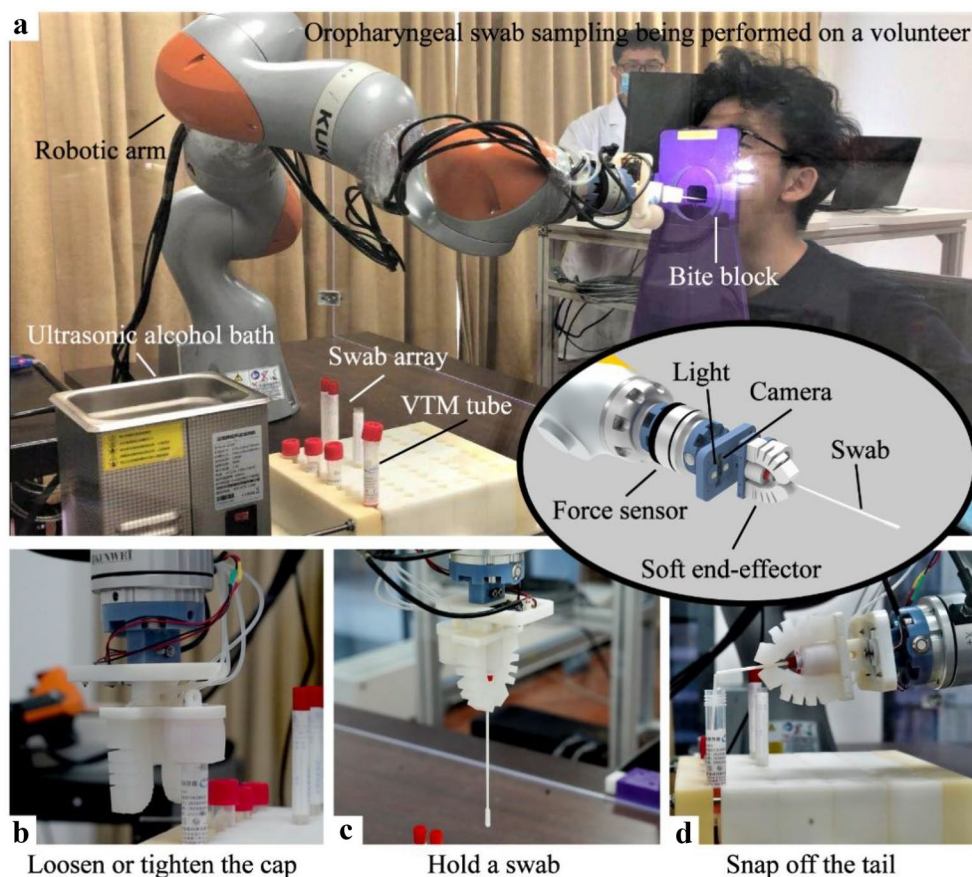


**Figure 1** Proposed robotic oropharyngeal swab sampling system with soft end-effectors: (a) Robotic swab-sampling system collecting samples from a volunteer (inset: soft end-effector holding an oropharyngeal swab), (b) Soft-end effector loosening or tightening the VTM tube cap, (c) Soft-end effector holding a swab and preparing for sample collection, (d) Soft-end effector snapping off the swab tail

can proceed successfully, from loosening and tightening the medium cap, holding the swab, and conducting sampling, to snapping off the swab tail and sterilizing itself. Using an industrial collaborative robotic arm, we integrated a soft end-effector, force sensor, camera, lights, and remote-control stick, and developed a robotic oropharyngeal swab sampling system. We tested this sampling system on 20 human volunteers. Digital PCR assay results for the collected specimens' RNase P RNA gene absolute copy numbers show that our system successfully collected a sufficient number of cells from the pharyngeal wall for respiratory disease diagnosis.

This study makes two novel contributions. First, we propose a light-weight and compact “enveloping” fabric-reinforced strain-limiting actuator, with features including stiffness variability and fault tolerance. These features have rarely been investigated for similar designs. This device can tightly and stably grasp the swab cap, screw and unscrew the VTM tube cap, and snap off the swab tail. Second, this device uses a soft gripper for sampling. Based on the manual sampling process,

a specialized robotic sampling process was examined, and a corresponding control algorithm was designed to achieve operations such as grasping the swab and tightening and loosening the VTM caps.

## 2 Design and Characterization

### 2.1 Design of a Soft Robotic End-Effector

Various types of swabs are used in the market to test for respiratory infectious diseases (Figure 2(a)); some are packaged in a plastic tube with a cylindrical cap at the end while others are packaged in a plastic bag with no cap, and some come with separate VTM tubes while others do not. Some swabs are tightly housed in tubes and require a large force to extract them (e.g., >30 N). To fit the different types of swabs and VTM tubes, we designed several end-effectors (Figure 2(b) and (c)). Figure 2(b) shows a soft end-effector composed of two cylindrical actuators and two finger-actuators for handling swabs packaged in plastic tubes. Figure 2(c) shows a soft end-effector composed of a cylindrical actuator, a cylindrical



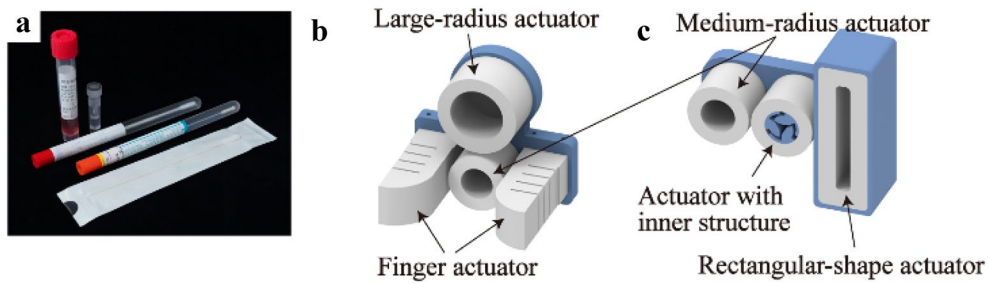


**Figure 2** Soft end effector designs: (a) Different types of swab packages, (b) Soft end-effector composed of two cylindrical actuators and two finger actuators, (c) Soft end-effector composed of a cylindrical actuator, a cylindrical actuator with inner rigid structure, and a rectangular actuator

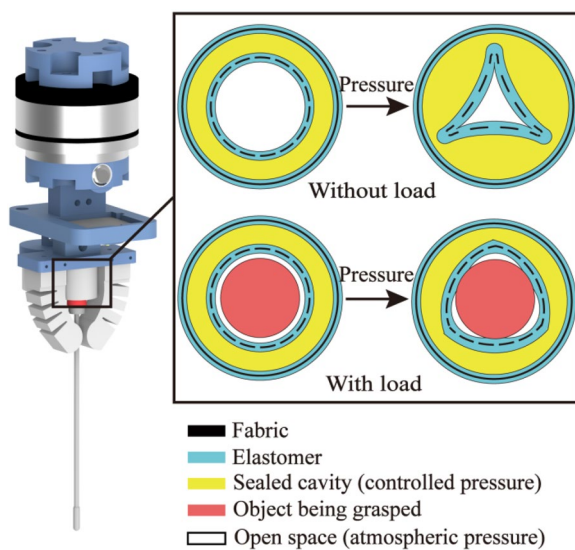


**Figure 3** Soft end effector integrated with force sensor, camera, and lights (enlarged inset: cross-sectional diagram of the gripping mechanism of the cylindrical actuator)

actuator with a rigid inner structure, and a rectangular actuator for handling swabs packaged in plastic bags.

Figure 3 presents a fabric-reinforced elastomeric cylindrical actuator with a closed and circumferentially distributed cavity, providing a key design for grasping, holding, and manipulating a swab. The outer wall of the actuator has a continuous sheet of fabric embedded in it. The inner wall is embedded with a sheet of fabric with slits oriented along the cylinder. When the closed cavity is pneumatically pressurized, the outer wall undergoes negligible deformation owing to the continuously embedded fabric, while the inner wall deforms inward. The slits in the cut fabric limit the axial strain, while allowing radial and circumferential strain. When an object is present in the center of the cylindrical actuator, the pressure difference drives the inner wall to enclose it tightly and stably, with a distributed force (Figure 3).

This fabric-reinforced cylindrical actuator can be designed to have any form or dimension to fit the different objects being grasped. Figure 4 shows five types

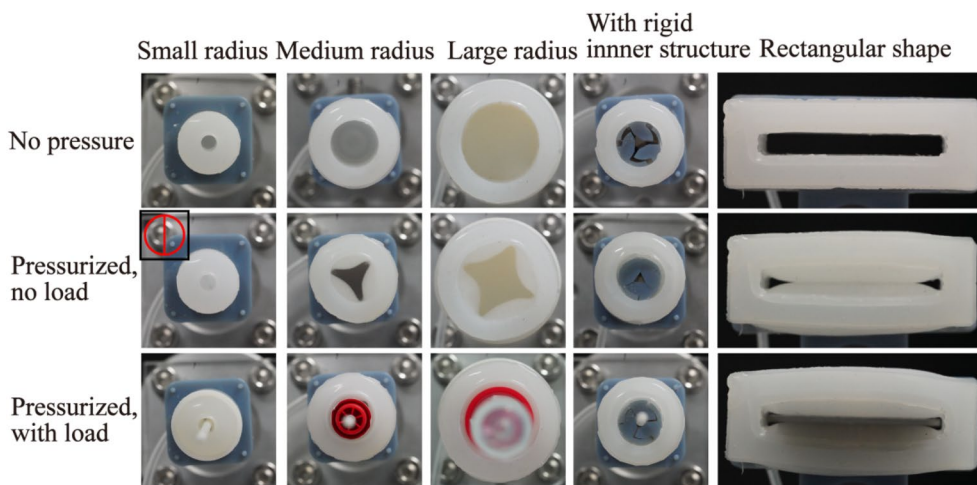


**Figure 4** Five types of cylindrical actuators in three states: no pressure, pressurized with no load, and pressurized with load

of actuators. The first three have circular cavities with different opening dimensions, for grasping cylindrical objects of different diameters. They are designed to grasp a bald swab (one with no cap), a swab with an end cap, and a VTM tube cap, respectively.

An important feature of the cylindrical actuator is that as the pressure difference at the inner wall reaches a critical value, it buckles circumferentially into a noncircular shape, and the buckling pattern varies with the dimensions of the actuator (Figures 3, 4, and Additional file 1). Buckling of thin-walled cylindrical shells under pressure has been extensively studied: the critical buckling pressure  $P_c$  depends on the inner wall geometry and on the material's Young's modulus,  $E$  [48]:

$$P_c = 0.883a_p E \left(\frac{r}{l}\right) \left(\frac{t}{r}\right)^{2.5}, \quad (1)$$

where  $r$ ,  $l$ ,  $t$  are the radius, height, and thickness of the inner wall, respectively, and  $a_p$  is a geometry-dependent constant ranging from 1 to 2. In our proposed design, the inner-wall thickness is much smaller than its radius ( $t \ll r$ ), and the critical pressure  $P_c$  is low; as a result, the circumference buckles at a relatively low pressure.

The buckling form or wavenumber  $N$  also depends on the geometry:

$$N = 3.12b_p \left(\frac{r}{l}\right)^{0.5} \left(\frac{r}{t}\right)^{0.25}, \quad (2)$$

where  $b_p$  is a geometry-dependent constant ranging from 0.6 to 1.1. From Eq. (2), we can see that wavenumber increases with the radius, consistent with what we found for our design. The small-radius actuator buckles into a two-segment strip, the medium one (inner diameter 14 mm) into a triangle, and the large one (inner diameter 23 mm) into a quadrilateral shape. This instability pattern is important for achieving stable grasping. If a two-segment strip is formed, the object is grasped from two opposing sides, leading to insufficient grasping force in the vertical direction. When triangular, quadrilateral, or even higher-order buckling occurs, forces are exerted on the object from more directions, so that grasping stiffness and stability from all directions.

To overcome the insufficient stiffness resulting from the two-segment buckling of the small actuator (for grasping a bald swab), we designed a fourth type of end effector with a rigid skeleton inside the cylindrical column (Figure 4). The rigid skeleton comprises three parts that form a small triangle when squeezed by the inner wall, grasping the thin rod of the bald swab (Additional file 2). Finally, a fifth type of end-effector was designed to handle non-cylindrical objects such as swabs packaged within a plastic bag. The rectangular end effector

holds the plastic bag tightly and removes it from the swab (Additional file 2).

For the different types of swab packages, we combined multiple actuators (Figure 2(b, c)) and bonded them onto a base structure to connect them with the rest of the system (Figure 3). Figure 2(b) shows a soft end-effector composed of a medium-radius cylindrical actuator, a large-radius cylindrical actuator, and two bellow-structure bending actuators (finger-actuators). This is used for handling swabs packaged in plastic tubes with separate VTM tubes, such as those widely used for diagnosing infectious respiratory diseases in hospitals in China. We use this end effector as an example to demonstrate how it accomplishes swab-sampling. However, it is worth noting that our design can fit many other swab packages as well.

## 2.2 Specific Load and Stiffness Characterization

A complete oropharyngeal swab sampling process involves removing the swab from the packaging tube, loosening and tightening the VTM tube cap, sampling from the back of the throat, snapping off the swab tail, and discarding it. This procedure requires the end-effector, a soft and inherently highly pliable structure, to have sufficient grasping force ( $F$ ), torque ( $T$ ), and stiffness. The theoretical maximum grasping force and torque of the cylindrical actuators can be represented as:

$$F_{\max} = \mu \cdot P \cdot 2\pi r l, \quad (3)$$

$$T_{\max} = \mu \cdot P \cdot 2\pi r^2 l, \quad (4)$$

where  $\mu$  is the friction coefficient between the elastomer and object material,  $P$  is difference between sealed-cavity pressure and atmospheric pressure, and  $r$  and  $l$  are the cylinder radius and height, respectively. Based on Eqs. (3) and (4), at a certain pressure, the maximum force increases linearly with  $r$ , and the maximum torque increases with  $r^2$ . The ideal maximum force and torque are attained when the inner and outer diameters are equal. In practice, a small gap (1–2 mm) is retained between the object and the actuator to facilitate alignment.

We characterized the maximum axial force and torque of the cylindrical actuators for holding swabs or caps at different pressures (Figure 5(a) and (b)). Figure 5(a) shows the maximum gripping force, and Figure 5(b) shows the maximum gripping torque, as a function of pressure for the four types of cylindrical actuators. The results indicate that the maximum axial force and torque that the actuators can withstand increase with pressure at an approximately linear rate. At 140 kPa, the large-, medium-, small-radius cylindrical actuators, and the rigid structure actuator, can withstand axial forces

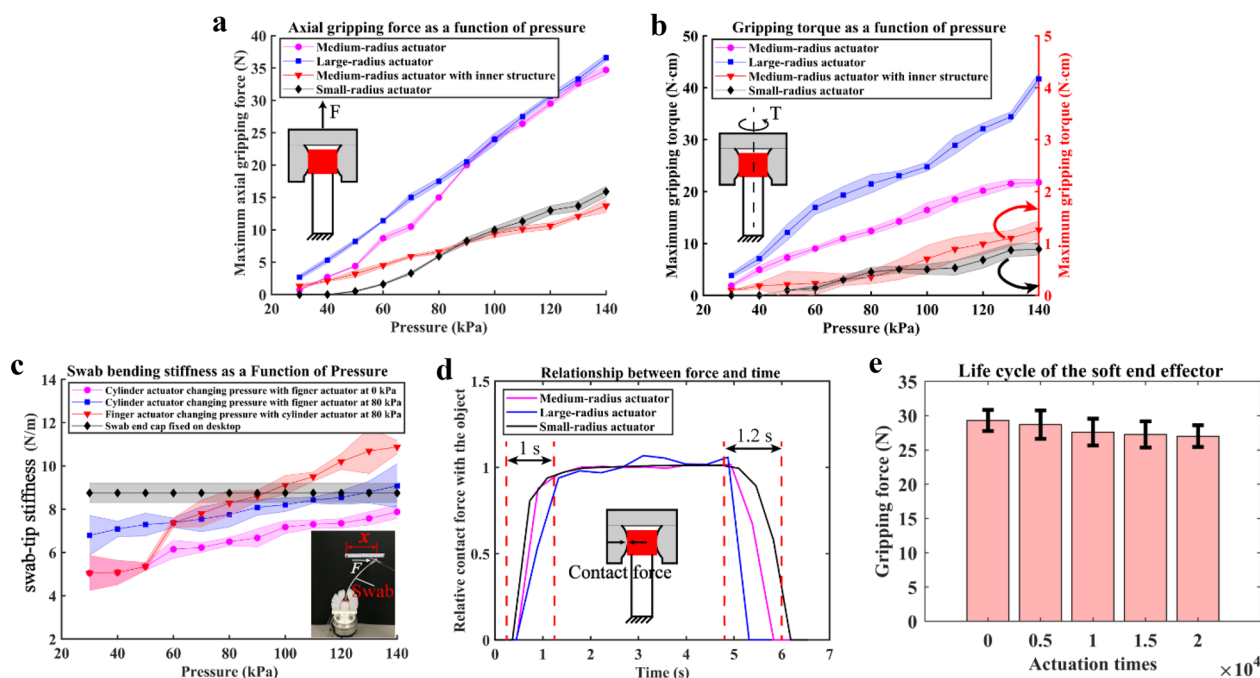


**Figure 5** Gripping force, torque, swab-tip stiffness, and speed characterization of the soft end-effectors

of 36.6 N, 34.7 N, 13.7 N, and 15.9 N, generating load-to-weight ratios of 215, 315, 196, and 118, respectively, without slipping. The large- and medium-radius cylindrical actuators can withstand torque of 41.68 N·cm and 21.76 N·cm, respectively, while the small cylindrical and rigid structure actuators can withstand 0.89 N·cm and 1.26 N·cm, respectively, without rotational slippage. The large-radius actuator exhibited the best torque-to-weight ratio of 24.52 N·m/kg. The high load-to-weight ratios and high torques that our proposed cylindrical actuators can withstand are critical in achieving complete automation of robotic swab-sampling. Specifically, the large-radius cylindrical actuator, with a maximum axial force of 36.6 N and maximum torque of 41.68 N·cm, can loosen and tighten the VTM tube; the medium-radius cylindrical actuator, with a maximum axial force of 34.7 N and maximum torque of 21.76 N·cm, can grasp and hold the swab end-cap and snap off the tail. In addition, the low weight of these elastomeric actuators means that they add negligible weight to the robotic arm that carries them. The key geometric parameters and mechanical performance parameters of the four types of cylindrical actuators are summarized in Table 1.

Swab-tip stiffness plays a key role in the sample collection process. We therefore characterized how our end-effector causes swab-tip stiffness to vary. Swab-tip stiffness (determined by applying a lateral force  $F$  and measuring tip displacement  $x$ ; tip stiffness  $k=F/x$ )

determines the pressure it applies when rubbing the back of the throat. Insufficient tip stiffness would cause the tip to collect too few cells, thus leading to low PCR-test sensitivity. Figure 5(c) illustrates the variation in swab-tip stiffness with changes in pressure caused by adjusting the pressure applied by the cylindrical and finger actuators. Because our actuator is composed of soft elastomers, swab-tip stiffness is lower when the swab is grasped by the actuator than when it is fixed on a rigid platform (baseline stiffness, 8.75 N/m, Figure 5(c), black line). Although increasing the actuator pressure significantly increases tip stiffness (Figure 5(c), magenta line), the actuator-gripped tip stiffness remains below the baseline even at a high pressure of 140 kPa, reaching 7.88 N/m. Thus, we used the two finger-actuators (Figure 2) to further enhance tip stiffness. By pressurizing the finger-actuators to 80 kPa, tip stiffness was increased to the baseline stiffness (Figure 5(c), blue line). By further increasing the finger-actuator pressure, an even higher stiffness (up to 10.88 N/m) could be obtained (Figure 5(c), red line). By adjusting the cylindrical actuator and finger-actuator pressures, we achieved variable swab-tip stiffness, ranging from 5.05 N/m to 10.88 N/m.

Next, we demonstrated that all of the cylindrical actuators have sufficient response speeds (response times of approximately 1 s, Figure 5(d)) during both actuation and de-actuation, controlled via a small pump and a few small solenoid valves. Figure 5(d) shows the time responses of

**Table 1** Geometric parameters and mechanical properties of the four types of cylindrical actuators

Parameters (unit)	Small-radius actuator	Medium-radius actuator	Large-radius actuator	Actuator with rigid inner structure
Inner shell I.D. (mm)	5	14	23	14
Inner shell O.D. (mm)	7.5	18	27	18
Outer shell I.D. (mm)	14	21.5	30.5	21.5
Outer shell O.D. (mm)	19	25	34.5	25
Cavity height (mm)	18	18	18	18
Total height (mm)	27	27	27	27
Total weight (g)	7	11	17	13.5
Grasped object diameter (mm)	2.5	12	20.5	2.5
Max. axial load at 140 kPa (N)	13.7	34.7	36.6	15.9
Max. torque at 140 kPa (N·cm)	0.89	21.76	41.68	1.26
Axial load/weight ratio at 140 kPa	196	315	215	118
Torque/weight ratio at 140 kPa (N·m/kg)	1.27	19.78	24.52	0.93

I.D.: Inner diameter; O.D.: Outer diameter

the three types of actuators obtained by measuring the internal contact force with the grasped objects. To date, we have demonstrated that our proposed soft end-effectors can accomplish all of the tasks required for automatic swab-sampling with sufficient load, stiffness, and speed.

Finally, we tested the lifecycle of the soft end-effector. Figure 5(e) shows the axial gripping forces at 100 kPa after 0, 5000, 10000, 15000, and 20000 repeated actuations to 100 kPa and deflation to 0 kPa. The soft end-effector functioned normally for at least 20000 actuations.

### 2.3 Fault Tolerance During Operation

During the swab sampling process, there are several tasks related to the precise control of robotic end-effector position and orientation. For example, to successfully remove the swab from the packaging tube, or grab the VTM tube cap, the axis of the robotic arm flange must be precisely aligned with the axes of the swab tube or VTM tube. These tasks can be challenging without sensory feedback and control, as the tubes have manufacturing and assembly errors. Soft end-effectors are capable of tolerating faults during this process. If the end flange of the robotic arm is misaligned (tilted or offset) in relation to the tube, the soft end-effector will adapt to the fault by deforming itself and will close around the end cap to complete the task. Figure 6(a) illustrates an example of axial-alignment error-tolerance, showing the axial forces during the process of aligning the cylindrical actuator and the VTM tube. The results show that our soft end-effector can tolerate up to 6 mm of tip displacement without destroying any part of the system, and the force caused by the deformation is less than 20 N, within the load capability

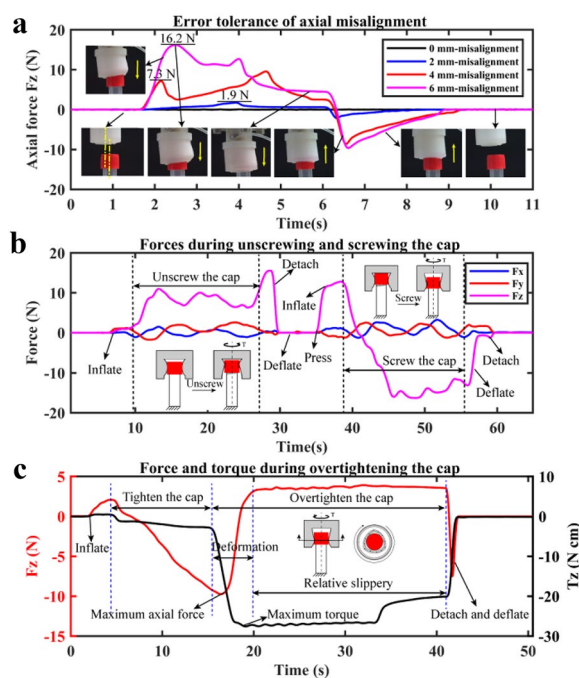


**Figure 6** Soft end-effector error-tolerance in handling VTM tubes

of most commercial robotic arms (Figure 6(a), Additional file 3).

Besides tolerating misalignment when screwing and unscrewing the cap, the soft end-effector exhibits fault tolerance that facilitates the control of the robotic arm. When a rigid end-effector is used to screw and unscrew the cap, rotational motion and precise proportional translational motion are required, whereas when using soft end-effectors, only rotation is required, and



translational displacement is achieved via soft end-effector deformation (insets in Figure 6(b)). Figure 6(b) shows the axial forces applied to the soft end effector due to axial deformation and slippage, illustrating tolerance of axial displacement when screwing and unscrewing the VTM tube caps. To loosen or tighten the cap, the end-effector grips the cap tightly, while the tube body is fixed on the table; the end-effector simply rotates, and the cap is screwed onto or unscrewed from the tube body (Additional file 4). The error tolerance of the robotic actuator significantly reduces the complexity of the algorithm for controlling the robotic arm and the positional accuracy requirement of the robotic arm.

Finally, the soft end-effector can tolerate overtightening of caps. Excessive relative motion between the tube body and tube cap causes shear deformation of the soft material and shear slippage (Figure 6(c) and Additional file 4).

### 3 Results and Discussion

#### 3.1 Implementation of Oropharyngeal Swab Sampling

Our robotic swab-sampling system comprises several subsystems and is located in two separate rooms (Figure 7(a)). In room one, there is a desk, chair, computer,

monitor, control stick, and foot pedal. In room two, there is a desk on which is placed a commercially available 7-DOF robotic arm (LBR iiwa from Kuka Robotics), swab array, sterilization bath, and dryer; beneath the desk is the controller for the robotic arm and the controller for the soft end-effector.

The visual and force data were collected using a camera (RER-USB13M02, Ruierweishi Company) and force sensor (KWR 75A, Kunwei Company), respectively, attached to the end of the robotic arm, and were remotely monitored by the doctor in room one using a host computer and monitor. The doctor's commands, entered using the computer, foot pedal (CFS-01, Neiluo Dianqi Company), or control stick (SMC35, Shenzhen Longfly Company), are transferred through data cables to the controllers at a sampling frequency of 5 Hz. The controllers control the robotic arm, the soft end-effector, and the other elements to complete the sampling process (Figure 7(b)). The block diagram in Figure 7(b) shows the data and action flows of the robotic swab-sampling system.

There are two controllers in the system (Figure 7(b)). One controls the KUKA robotic arm, and the other controls the soft end-effector. The robotic arm is controlled

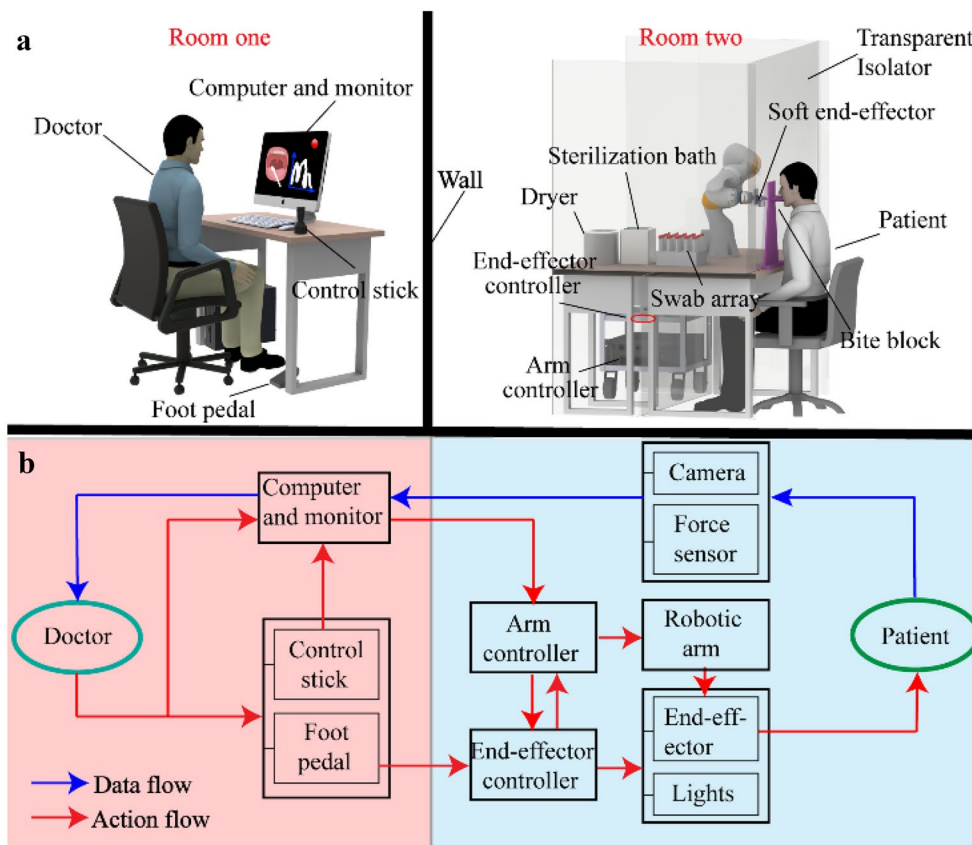


Figure 7 Robotic oropharyngeal swab-sampling system



by the commercial KUKA control box provided with the arm; based on the information in the LBR iiwa brochure, the positional accuracy of our end-effector is  $\pm 0.1$  mm. The end-effector controller consists of a pump, five solenoid valves, and a control board (Modbus RTU Protocol); the controller software was self-developed in C++ to send instructions to the control board (Figure 8). The five valves are two-position three-way valves. Valves 1 and 2 are diverter valves (Figure 8(a)). The compressed air from the pump flows into valve 1. At low pressure, the air flowing out of valve 1 flows into valve 3. At high pressure, the air flowing out of valve 1 flows into valve 2. The working principle of valve 2 is the same as that of valve 1. At a high pressure, the air flows through valves 3, 4, and 5 to inflate the corresponding actuators, while at a low pressure, the air in the corresponding actuators flows to the atmosphere through valves 3, 4, and 5 (Figure 8(a)). This control system enables each actuator to be independently controlled during both inflation and deflation, enabling the three actuators to be in various combinations of states to complete the various tasks. Our implementation of the swab-sampling process includes many different combinations of states for the pump and valves. The five valves and the pump are connected to a Modbus RTU control board, which connects to the arm controller and foot pedal via an RS485 serial communication port (Figure 8(b)). The arm controller sends commands to the

Modbus RTU control board to control the state of the pump and valves. The foot pedal sends commands to the arm controller via the control board to start and stop the movement of robotic arm. The control box is compact, and all of the elements are contained within a customized protective box (Figure 8(c)).

In our proposed system, the doctor and patient (or potential patient) are isolated in space, thereby reducing the doctor’s risk of becoming infected as a result of contact with someone carrying the virus. The sampling process is shown in Figure 9(a). When the contact force between the swab and the oropharynx reaches 0.5 N (trigger force), the robotic arm will stop moving forward and start sampling. The force-feedback-triggered sampling process ensures that, regardless of far back from the mouth the pharyngeal wall is, the swab can always press and rub along the wall and sample at the correct location on the wall. The robotic arm has built-in overload protection throughout the process: If it encounters a collision force exceeding 20 N, it will immediately stop moving. In addition, the doctor can press the emergency stop button to prevent the robot from moving. These two safety features ensure that the robot will not harm the patient. To avoid injury in extreme situations in which both of these safety features fail, we have limited the speed of the robotic arm’s tool center point (TCP) to 2 m/s, which is associated with a head injury criterion (HIC) value of 25,

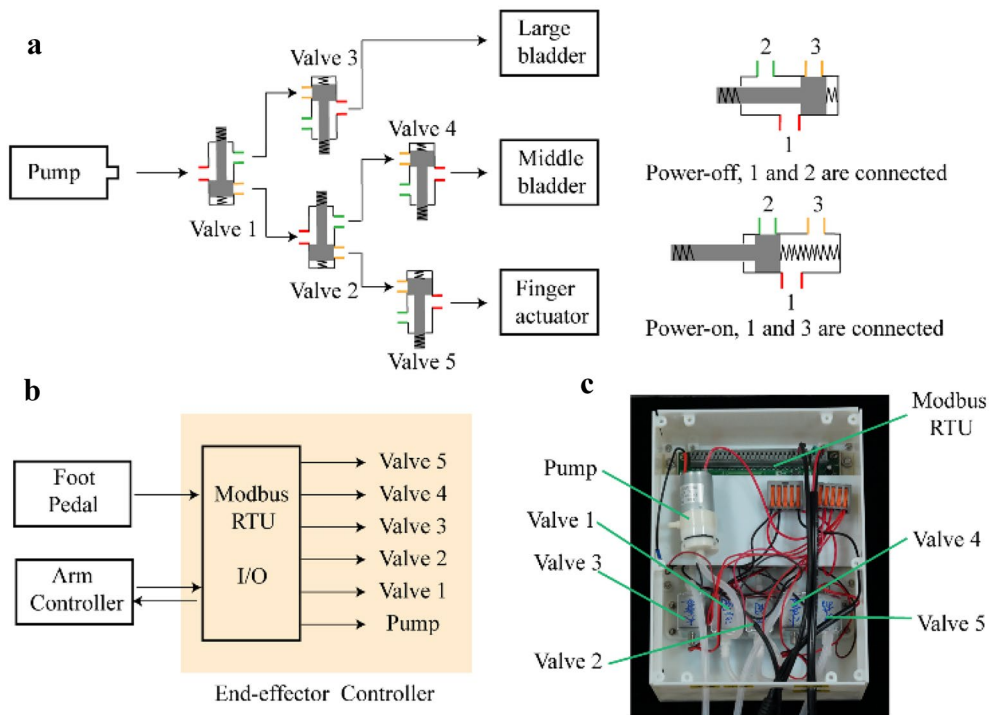


**Figure 8** Control system of the soft end-effector

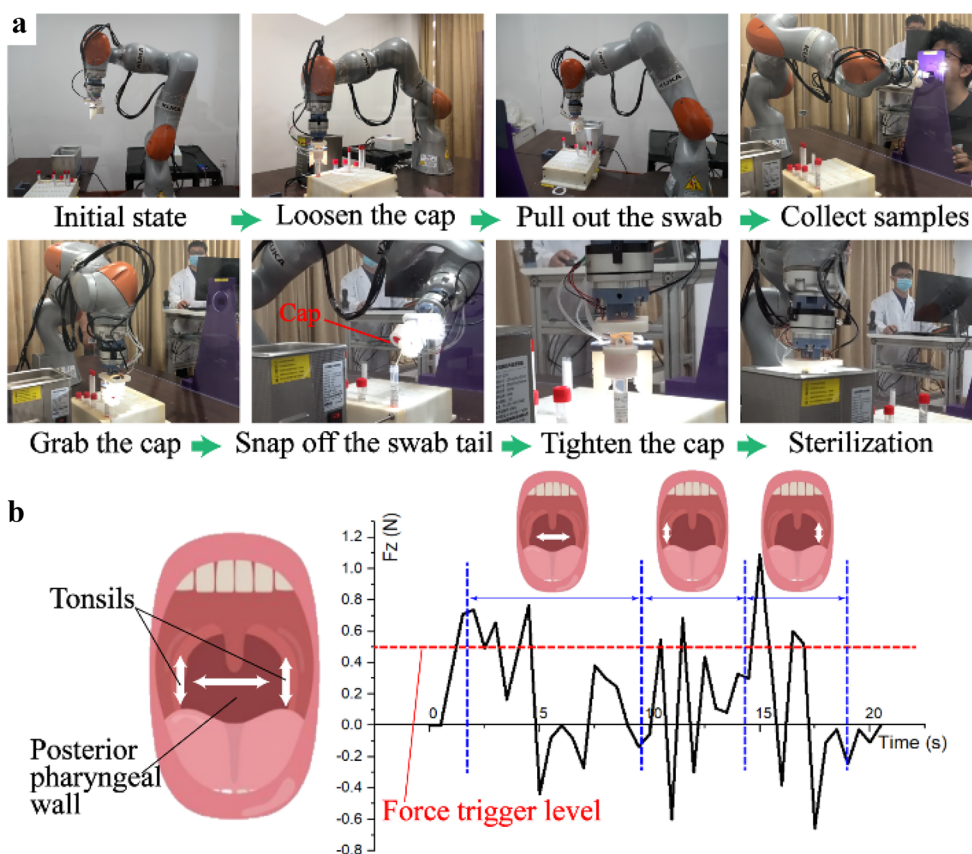


**Figure 9** Swab sampling process

thereby satisfying the  $HIC < 650$  safety rule [49]. The HIC is a standard index of injury severity [50].

### 3.2 Human Testing of Manual and Robotic Swab-Sampling

The human studies were reviewed and approved by the Institutional Review Board of Tsinghua University. Twenty-one volunteers ranging in age from 23 to 36 years, height 158 cm to 183 cm, and weight 45 kg to 95 kg, were recruited for these tests. All of the volunteers were physically and mentally healthy. The 21 volunteers were divided into two groups: 11 were swab-sampled by a doctor on day one and by our robotic system on day two; the other ten were swab-sampled by the robot on day one and by a doctor on day two. The two-day process ensured that the epithelial cells on the posterior pharyngeal wall were able to recover.

Before testing, the volunteers were informed about the potential hazards associated with the swab-sampling process, such as throat reflex, vomiting, and foreign body sensation. For doctor-conducted sampling, each volunteer sat on a chair and opened his or her mouth. The doctor used a tongue depressor to assist in the sampling process. Using an oropharyngeal swab,

the doctor swabbed the back wall of the throat by rubbing 3–5 times back and forth, and then rubbing along the sidewalls of the tonsils 1–2 times for each tonsil. The doctor then placed the swab into the VTM tube, snapped the tail off, and screwed the cap on.

For robotic sampling, each volunteer was provided with a disposable positioning bite block. The volunteer bit into the bite block in order to be sampled. The robot completed the remainder of the sampling process under remote-control by a doctor. Additional file 5 shows a typical video of a volunteer during testing. Figure 9(b) shows the typical contact-force evolution as the swab is being rubbed along the posterior pharyngeal wall and tonsils.

Of the 21 participants, 20 successfully completed both manual and robotic sampling, and one participant withdrew after day 1 because of a sore throat after manual testing. On each day, we collected 10 doctor-sampled and 10-robot-sampled oropharyngeal samples. Most of the 20 participants who completed both tests felt normal when they were sampled using the robotic system. A few experienced slight discomfort or gagging reflex, which are normal reactions to successful sampling.

### 3.3 Digital PCR Testing Results and Analysis

Digital polymerase chain reaction (Digital PCR) is a quantitative analysis technique increasingly used in clinical diagnosis, especially for the study of human pathogenic viruses [51, 52]. Digital PCR allows precise detection and quantification of the number of nucleic acids [53]. It has good accuracy and reproducibility and can achieve absolute quantitative analysis. The RNase P gene occurs widely in human cells [54]. Here, we used a digital PCR assay to determine the absolute RNase P gene copy number in the oropharyngeal samples, and compared the effectiveness of the two sampling methods. The absolute RNase P gene copy numbers for each participant, based on the 40 oropharyngeal samples collected, are shown in Figure 10(a).

We divided the 40 samples into four groups: Manual testing on day 1, robotic testing on day 1, manual testing on day 2, and robotic testing on day 2. We calculated the mean and standard deviation of each group’s absolute RNase P gene copy number (Figure 10(b)); these findings reveal that robotic sampling generated higher average absolute copy numbers than manual sampling, on both days. To further investigate the effects of robotic and manual sampling, as well as the effects of the testing

sequence, we performed a repeated two-way ANOVA on the 40 absolute copy numbers. This revealed non-significant effects of the sampling method (robot vs. doctor) ( $F_{(1, 39)}=1.71, p=0.1997$ ) and sampling sequence ( $F_{(1, 39)}=2.27, p=0.1402$ ) on absolute copy number. The sampling method–sequence interaction was also non-significant ( $F_{(1, 39)}=0.33, p=0.5684$ ). From these results, based on PCR assay of absolute RNase P gene copy number, we can conclude that the robotic system achieved oropharyngeal swab-sampling results that were not significantly different from those obtained via manual testing. This statistical analysis confirms the functionality and effectiveness of the proposed robotic oropharyngeal swab-sampling system using soft end-effectors.

The use of robots can greatly reduce a doctor’s workload and mental stress, by making it unnecessary for them to perform sampling and face the patient in person. Instead, the doctor can remain in a separate room, control the computer, and monitor the process of sampling. This substantially reduces the doctor’s risk of becoming infected during sampling, and effectively reduces their workload.

### 4 Conclusions

- (1) In this paper, we have presented a pharyngeal swab-sampling system based on an “enveloping” soft actuator, explored the sampling process, and applied the system for pharyngeal swab-sampling. We have implemented complete oropharyngeal robotic swab-sampling using a soft end-effector. To the best of our knowledge, this has not been achieved previously.
- (2) We have automated the necessary processes, such as picking up the swabs and placing the samples into VTM tubes, as well as sterilization and disposal. This automation enables the patient and doctor to remain isolated while the sampling is accomplished effectively.
- (3) The results of our comparative digital PCR assay of 20 volunteers’ oropharyngeal samples, obtained via robotic and manual sampling, demonstrate that our implementation has promising application potential. We hope that this trial of automatic sampling (assisted by force and visual feedback) of both the posterior pharyngeal wall and the tonsils will lay the first step in answering the difficult question of how a robot should perform oropharyngeal swab sampling. In this time of the infectious respiratory disease pandemic, we look forward to seeing the mass application of such systems worldwide, thereby protecting more people, especially nurses and doctors, from viral infections.

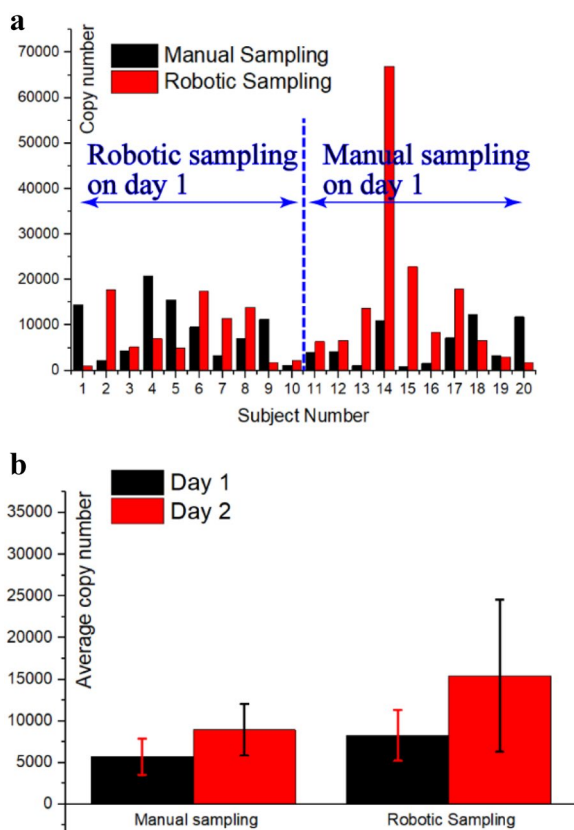


Figure 10 Human testing results

- (4) The soft end-effector exhibited excellent performance. It has the flexibility to be designed with different forms to fit various types of swab packages. It has a large load-to-weight ratio and exhibits fault tolerance and variable swab stiffness during sampling.
- (5) The capability of the proposed soft end-effectors to handle tubes and caps demonstrates their potential for use in many other scenarios, such as in manufacturing and assembly lines. For robotic sampling, a specifically designed robotic arm (perhaps a soft or hybrid arm) might be a better option to replace the current commercial arm and reduce costs, save space, and increase time efficiency. A more advanced force-feedback algorithm for use during sampling could be developed to further increase sampling efficiency and mitigate the discomfort of the person being tested during sampling.

## Supplementary Information

The online version contains supplementary material available at <https://doi.org/10.1186/s10033-024-01009-5>.

**Additional file 1.** Performance of different types of cylindrical actuators.

**Additional file 2.** Rectangular actuator taking swab out of a plastic package.

**Additional file 3.** Error tolerance demonstration of the soft end effector enclosing a VTM tube with misalignment.

**Additional file 4.** Error tolerance demonstration of the soft end effector screwing and unscrewing a VTM tube.

**Additional file 5.** Complete robotic oropharyngeal swab sampling on a volunteer.

## Acknowledgements

We would like to thank Prof. Xiangjun Zhang, Prof. Fugui Xie, Prof. Timing Qu, Dr. Zuobo Wu, Dr. Ruihao Li, Zhonghan Lin, Lin Sheng, Xiujun Zhai, Liang Yu, and Xuguang Dong for their kind help and great inspiration in this work.

## Authors' Contributions

JY, JW, and HZ proposed and designed the research; JY, GY, and JL provided medical advice and design; YC, QS, XL, and HZ designed and built the soft end effector; WY wrote the code for controlling the robotic arm; JL conducted the digital PCR assay; DW, GY, and XZ designed the bite block; YC, WY, JL, and HZ conducted experiments; YC, JL, and HZ analyzed the data; YC and HZ wrote the paper. All authors read and approved the final manuscript.

## Funding

Supported by National Natural Science Foundation of China (Grant Nos. 52222502, 92048302, and 51975306), Research Project of State Key Laboratory of Mechanical System and Vibration of China (Grant No. MSV201904), and Emergency Research Project for COVID-19 from Institute for Precision Medicine of Tsinghua University of China.

## Data Availability

The data that support the findings of this study are available within the article or its supplementary materials.

## Declarations

### Competing Interests

The authors declare no competing financial interests.

Received: 30 May 2022 Revised: 9 January 2024 Accepted: 23 February 2024

Published online: 21 March 2024

## References

- [1] A Clark, M Jit, C Warren-Gash, et al. Global, regional, and national estimates of the population at increased risk of severe COVID-19 due to underlying health conditions in 2020: A modelling study. *Lancet Glob. Health*, 2020, 8(8): 1003–1017.
- [2] E Mahase. Coronavirus covid-19 has killed more people than SARS and MERS combined, despite lower case fatality rate. *BMJ*, 2020, 368: m641.
- [3] COVID-19 coronavirus pandemic database. <https://www.worldometers.info/coronavirus>. Accessed 7 May 2022.
- [4] C Huang, Y Wang, X Li, et al. Clinical features of patients infected with 2019 novel coronavirus in Wuhan, China. *Lancet*, 2020, 395(10223): 497–506.
- [5] W Guan, Z Ni, Y Hu, et al. Clinical characteristics of coronavirus disease 2019 in China. *N. Engl. J. Med.*, 2020, 382: 1708–1720.
- [6] L Zou, F Ruan, M Huang, et al. SARS-CoV-2 viral load in upper respiratory specimens of infected patients. *N. Engl. J. Med.*, 2020, 382(12): 1177–1179.
- [7] M J Loeffelholz, Y Tang. Laboratory diagnosis of emerging human coronavirus infections—the state of the art. *Emerg. Microbes Infect.*, 2020, 9(1): 747–756.
- [8] W Wang, Y Xu, R Gao, et al. Detection of SARS-CoV-2 in different types of clinical specimens. *Jama*, 2020, 323(18): 1843–1844.
- [9] Z Xie, B Chen, J Liu, et al. A tapered soft robotic oropharyngeal swab for throat testing: A new way to collect sputa samples. *IEEE Robotics & Automation Magazine*, 2021, 28(1): 90–100.
- [10] J Chen, H Lu, G Melino, et al. COVID-19 infection: The China and Italy perspectives. *Cell Death Dis.*, 2020, 11(6): 438.
- [11] P Winichakoon, R Chaiwarith, C Liwsrisakunet, et al. Negative nasopharyngeal and oropharyngeal swab does not rule out COVID-19. *J. Clin. Microbiol.*, 2020, 58(5): e00297–20.
- [12] S Wang, K Wang, R Tang, et al. Design of a low-cost miniature robot to assist the COVID-19 nasopharyngeal swab sampling. *IEEE Transactions on Medical Robotics and Bionics*, 2021, 3(1): 289–293.
- [13] A D Lallo, R Murphy, R Krieger, et al. Medical robots for infectious diseases: Lessons and challenges from the COVID-19 pandemic. *IEEE Robotics & Automation Magazine*, 2021, 28(1): 18–27.
- [14] H Su, A D Lallo, R Murphy, et al. Physical human–robot interaction for clinical care in infectious environments. *Nat. Mach. Intell.*, 2021, 3: 184–186.
- [15] R L Truby, W Michael, A K Grosskopf, et al. Soft somatosensitive actuators via embedded 3D printing. *Adv. Mater.*, 2018, 30: 1706383.
- [16] F Ilievski, A D Mazzeo, R F Shepherd, et al. Soft robotics for chemists. *Angewandte Chemie*, 2011, 50(8): 1890–1895.
- [17] H Zhao, K O'Brien, S Li, et al. Optoelectronically innervated soft prosthetic hand via stretchable optical waveguides. *Sci. Robot.*, 2016, 1(1): eaai7529.
- [18] D Rus, M T Tolley. Design, fabrication and control of soft robots. *Nature*, 2015, 521: 467–475.
- [19] L Lindenroth, A Soor, J Hutchinson, et al. Design of a soft, parallel end-effector applied to robot-guided ultrasound interventions. *Proceedings of the IEEE International Conference on Intelligent Robots and Systems*, Vancouver, BC, Canada, September 24–28, 2017: 3716–3721.
- [20] P Polygerinos, Z Wang, K C Galloway, et al. Soft robotic glove for combined assistance and at-home rehabilitation. *Rob. Auton. Syst.*, 2015, 73: 135–143.
- [21] C Laschi, B Mazzolai, M Cianchetti. Soft robotics: Technologies and systems pushing the boundaries of robot abilities. *Sci. Robot.*, 2016, 1(1): eaai3690.
- [22] D Mura, M Barbarossa, G Dinuzzi, et al. A soft modular end effector for underwater manipulation: A gentle, adaptable grasp for the ocean depths. *IEEE Robot. Autom. Mag.*, 2018, 25(4): 45–56.



- [23] M Cianchetti, M Calisti, L Margheri, et al. Bioinspired locomotion and grasping in water: The soft eight-arm OCTOPUS robot. *Bioinspir. Biomim.*, 2015, 10(3): 035003.
- [24] E W Hawkes, H Jiang, D L Christensen, et al. Grasping without squeezing: Design and modeling of shear-activated grippers. *IEEE Trans. Robot.*, 2018, 34(2): 303–316.
- [25] Z Xie, A G Domel, N An, et al. Octopus arm-inspired tapered soft actuators with suckers for improved grasping. *Soft Robot.*, 2020, 7(5): 639–648.
- [26] R Deimel, O Brock. A novel type of compliant and underactuated robotic hand for dexterous grasping. *Int. J. Rob. Res.*, 2016, 35(1-3): 161–185.
- [27] Y Wu, J K Yim, J Liang, et al. Insect-scale fast moving and ultrarobust soft robot. *Sci. Robot.*, 2019, 4(32): eaax1594.
- [28] G Gu, J Zou, R Zhao, et al. Soft wall-climbing robots. *Sci. Robot.*, 2018, 3(25): eaat2874.
- [29] K J Cho, J S Koh, S Kim, et al. Review of manufacturing processes for soft biomimetic robots. *Int. J. Precis. Eng. Manuf.*, 2009, 10(3): 171–181.
- [30] Y Chen, H Zhao, J Mao, et al. Controlled flight of a microrobot powered by soft artificial muscles. *Nature*, 2019, 575: 324–329.
- [31] J Shintake, V Cacucciolo, D Floreano, et al. Soft robotic grippers. *Adv. Mater.*, 2018, 30: e1707035.
- [32] J Hughes, U Culha, F Giardina, et al. Soft manipulators and grippers: A review. *Front. Robot. AI*, 2016, 3: 69.
- [33] K C Galloway, K P Becker, B Phillips, et al. Soft robotic grippers for biological sampling on deep reefs. *Soft Robot.*, 2016, 3(1): 236–243.
- [34] E Brown, N Rodenberg, J Amend, et al. Universal robotic gripper based on the jamming of granular material. *Proc. Natl. Acad. Sci. U.S.A.*, 2010, 107(44): 188096–18814.
- [35] J Shintake, S Rosset, B Schubert, et al. Versatile soft grippers with intrinsic electroadhesion based on multifunctional polymer actuators. *Adv. Mater.*, 2016, 28: 231–238.
- [36] K W O'Brien, P A Xu, D J Levine, et al. Elastomeric passive transmission for autonomous force-velocity adaptation applied to 3D printed prosthetics. *Sci. Robot.*, 2018, 3(23): eaau5543.
- [37] J R Amend, E Brown, N Rodenberg, et al. A positive pressure universal gripper based on the jamming of granular material. *IEEE Trans. Robot.*, 2012, 28(2): 341–350.
- [38] N R Sinatra, C B Teeple, D M Vogt, et al. Ultragentle manipulation of delicate structures using a soft robotic gripper. *Sci. Robot.*, 2019, 4(33): eaax5425.
- [39] S Li, J J Stampfli, H J Xu, et al. A vacuum-driven origami “magic-ball” soft gripper. *Proceedings of the IEEE International Conference on Robotics and Automation*, Palais des congrès de Montreal, Montreal, Canada, May 20–24, 2019: 7401–7408.
- [40] Soft gripper. <https://www.softroboticsinc.com/>. Accessed 7 May 2022.
- [41] Soft gripper flexible food-grade robot gripper. <https://onrobot.com/en/products/soft-gripper>. Accessed 7 May 2022.
- [42] D Wang, X Wu, J Zhang, et al. A pneumatic novel combined soft robotic gripper with high load capacity and large grasping range. *Actuators*, 2022, 11(3). <https://doi.org/10.3390/act11010003>.
- [43] G Yang, Bradley, J Nelson, et al. Combating COVID-19—The role of robotics in managing public health and infectious diseases. *Sci. Robot.*, 2020, 5(40): eabb5589.
- [44] D Sui, T Wang, S Zhao, et al. An enveloping soft gripper with high-load carrying capacity: Design, characterization and application. *IEEE Robot. Autom. Lett.*, 2022, 7(1): 373–380.
- [45] Y Hao, S Biswas, E W Hawkes, et al. A multimodal, enveloping soft gripper: shape conformation, bioinspired adhesion, and expansion-driven suction. *IEEE Trans. Robot.*, 2021, 37(2): 350–362.
- [46] H Li, J Yao, P Zhou, et al. High-load soft grippers based on bionic winding effect. *Soft Robot.*, 2019, 6(2): 276–288.
- [47] H Li, J Yao, C Wei, et al. An untethered soft robotic gripper with high payload-to-weight ratio. *Mech. Mach. Theory*, 2020, 158: 104226.
- [48] N Yamaki. *Buckling of circular cylindrical shells under fundamental loads, in elastic stability of circular cylindrical shells*. Elsevier, 1984.
- [49] S Haddadin, A S Alin, H Gerd. Safety evaluation of physical human-robot interaction via crash-testing. *In Robotics: Science and systems*, 2007, 3: 217–224.
- [50] J Versace. A review of the severity index. *Proceedings of the 15th Stapp Car Crash Conference*, 1971: 771–796.
- [51] J T Huang, Y J Liu, J Wang, et al. Next generation digital PCR measurement of hepatitis B virus copy number in formalin-fixed paraffin-embedded hepatocellular carcinoma tissue. *Clin. Chem.*, 2015, 61(1): 290–296.
- [52] I Giovannelli, N Ciccone, G Vaggelli, et al. Utility of droplet digital PCR for the quantitative detection of polyomavirus JC in clinical samples. *J. Clin. Virol.*, 2016, 82: 70–75.
- [53] B Vogelstein, K W Kinzler. Digital PCR. *Proc. Natl. Acad. Sci. U.S.A.*, 1999, 96: 9236–9241.
- [54] S Dube, J Qin, R Ramakrishnan. Mathematical analysis of copy number variation in a DNA sample using digital PCR on a nanofluidic device. *PLoS One*, 2008, 3(8): e2876.

**Yafeng Cui** born in 1995, received his PhD degree from *Department of Mechanical Engineering, Tsinghua University, China*, in 2023. He received his bachelor degree from *Electronic Science and Technology of China, China*, in 2018. His research interests include soft robotics, soft grippers, and robotic design.

**Wenjie Yu** is currently an engineer at *Beijing Huakang Tongbang Technology Company, China*.

**Jingjing Li** is currently a doctor at *Department of Otorhinolaryngology, Beijing Tsinghua Changgung Hospital, China*.

**Qi Shao** is currently a PhD candidate at *Department of Mechanical Engineering, Tsinghua University, China*.

**Ding Weng** is currently an associate professor at *Department of Mechanical Engineering, Tsinghua University, China*.

**Guoping Yin** is currently a doctor at *Department of Otorhinolaryngology, Beijing Tsinghua Changgung Hospital, China*.

**Xiaohao Zhang** is currently an engineer at *Tianjin Research Institute for Advanced Equipment, Tsinghua University, China*.

**Xinjun Liu** is currently a professor at *Department of Mechanical Engineering, Tsinghua University, China*.

**Jingying Ye** is currently a professor at *Department of Otorhinolaryngology, Beijing Tsinghua Changgung Hospital, School of Clinical Medicine, Tsinghua University, China*.

**Jiadao Wang** is currently a professor at *Department of Mechanical Engineering, Tsinghua University, China*.

**Huichan Zhao** is currently an associate professor at *Department of Mechanical Engineering, Tsinghua University, China*. Her research interests include soft robotics, soft sensors and actuators, bioinspired robots, robotic manipulation and locomotion, etc.